Cav03-GS-2-013

Fifth International Symposium on Cavitation (CAV2003)
Osaka, Japan, November 1-4, 2003

REDUCED-ORDER MODELING OF DIFFUSIVE EFFECTS ON THE DYNAMICS OF BUBBLES

Al Preston **Tim Colonius***
Christopher E. Brennen

Division of Engineering and Applied Science
California Institute of Technology
Pasadena, CA 91125
email: colonius@caltech.edu

ABSTRACT

The Rayleigh-Plesset equation and its extensions have been used extensively to model spherical bubble dynamics, yet radial diffusion equations must be solved to correctly capture damping effects due to mass and thermal diffusion. The latter are too computationally intensive to implement into a continuum model for bubbly cavitating flows, since the diffusion equations must be solved at each position in the flow. The goal of the present research is to derive a reduced-order model that accounts for thermal and mass diffusion. Motivated by results of applying the Proper Orthoganal Decomposition to data from full radial computations, we derive a model based upon estimates of the average heat and mass transfer coefficients. The model captures the damping effects of the diffusion processes in two ordinary differential equations, and gives better results than previous models.

INTRODUCTION

Detailed computations of forced and oscillating bubbles including heat and mass diffusion show that the assumptions of polytropic behavior, constant vapor pressure, and an effective liquid viscosity do not accurately account for diffusive damping and thus do not accurately capture bubble dynamics (Prosperetti et al. 1988, Watanabe & Prosperetti 1994, Matsumoto & Takemura 1994, Kameda & Matsumoto 1996). While the full bubble computations are readily performed for single bubbles, they are too expensive to implement into continuum models of complex bubbly flows where the radial diffusion equations would have to be solved at each grid point. Therefore reduced-order models that accurately capture diffusive effects are needed.

Previous models that account for thermal diffusive effects include the models of Prosperetti (1991) valid near either the isothermal or adiabatic limits, and the model of Storey & Szeri (2001), which switches between isothermal and adiabatic behavior depending upon relative time scales. However, these approaches are unable to correctly capture the thermal damping over a range of bubble responses (Preston et al. 2002*a*). Toegel et al. (2000) proposed a model that estimated the mass and thermal energy fluxes out of the bubble by using an estimation of the diffusive penetration length. This seems a reasonable approach for large bubbles, but can give poor results when the thermal penetration length approaches or exceeds the bubble radius.

We develop a reduced-order model based upon the homobarotropic formulation of Ichihara et al. (2000) (see also Nigmatulin et al. (1981) and Prosperetti et al. (1988)). We close the equations by using average heat and mass transfer coefficients which are estimated from linear analysis. The resulting model captures the diffusive effects with only two additional ordinary differential equations having to be integrated along with the Rayleigh-Plesset equation. Application of the *Proper Orthogonal Decomposition* (POD) to numerous full computations indicate the use of a single average transfer coefficient is reasonable, since most of the energy is captured by the first POD mode. In addition the POD results confirm that the estimation of the transfer coefficients from linear analysis is appropriate. Comparisons of the reduced order model to the full computations over a wide range of parameters indicate agreement that is superior to existing models.

REDUCED-ORDER MODEL

The reduced-order model is based on the simplified set of equations for a gas-vapor bubble with the internal pressure as-

*Address all correspondence to this author.

sumed to be spatially uniform. This assumption has been validated in detail (Lin et al. 2002) and enables the derivation of the following ordinary differential equation for the internal bubble pressure (Ichihara et al. 2000),

$$\frac{dp}{dt} = \frac{-3\gamma}{R}\left(p\frac{dR}{dt} - \frac{p_o}{Pe_g}\frac{1}{R}\frac{\partial T}{\partial y}\bigg|_{y=1} - \mathcal{R}_v T_w \dot{m}_v''\right). \quad (1)$$

The mass flux per unit area of vapor into the bubble is determined from reciprocal diffusion as,

$$\dot{m}_v'' = \frac{1}{Pe_{a-v}}\frac{\rho}{1-C}\frac{1}{R}\frac{\partial C}{\partial y}\bigg|_{y=1}, \quad (2)$$

where C is the mass concentration of vapor. These equations are coupled to the Rayleigh-Plesset equation [1] for the motion of the liquid,

$$R\frac{d^2R}{dt^2} + \frac{3}{2}\left(\frac{dR}{dt}\right)^2 + \frac{4}{ReR}\frac{dR}{dt} + \frac{2}{WeR} = p - p_\infty(t). \quad (3)$$

The variables in the above equations have been non-dimensionalized as $R = R'/R_o'$, $T = c_{pL}'T'/R_o'^2\omega_o'^2$, $p = p'/\rho_L'R_o'^2\omega_o'^2$, $\dot{m}_v'' = \dot{m}_v''/\rho_L'R_o'\omega_o'$, while $y = r'/R'(t)$ is the radial coordinate chosen to fix the bubble wall at $y = 1$. The non-dimensional perfect gas constant for the vapor is defined as $\mathcal{R}_v = \mathcal{R}_v'/c_{pL}'$, while the Reynolds number, Weber number and Peclet numbers for thermal and mass diffusivity, are given respectively as $Re = R_o'^2\omega_o'/\nu_L'$, $We = \rho_L'R_o'^3\omega_o'^2/S'$, $Pe_g = \rho_o'c_p'R_o'^2\omega_o'/k'$ and $Pe_{a-v} = R_o'^2\omega_o'/D'$, where ω_o' is the bubble natural frequency. The non-dimensional initial internal bubble pressure is computed from equilibrium of equation (3) as, $p_o = p_{\infty_o} + 2/We$, where p_{∞_o} is the non-dimensional ambient pressure.

The equations (1) through (3) are typically closed by the radial diffusion equations for the temperature and concentration distributions in the bubble. Rather than solve these computationally intensive partial differential equations we approximate the gradients at the bubble wall by employing average heat and mass transfer coefficients, β_T and β_C, such that,

$$\frac{\partial T}{\partial y}\bigg|_{y=1} \approx -\beta_T(\bar{T} - T_w), \quad (4)$$

$$\frac{\partial C}{\partial y}\bigg|_{y=1} \approx -\beta_C(\bar{C} - C_w). \quad (5)$$

[1] The present model can readily be used with other forms of the Rayleigh-Plesset equation, for example to include effects of liquid compressibility.

Here the subscript w denotes the value at the bubble wall, and the overbar denotes the volume average over the bubble. The choice of the approximations (4) and (5) have been motivated directly by results of the next section, where the Proper Orthoganal Decomposition has been applied to data from full bubble computations.

For the present situation, where variation in the liquid temperature is neglected, the temperature at the bubble wall is simply the initial temperature,

$$T_w = T_o, \quad (6)$$

while the wall concentration is determined by assuming the vapor pressure at the bubble wall is in equilibrium,

$$C_w = \frac{1}{1+\theta} \quad (7)$$

$$\theta = \frac{\mathcal{R}_v}{\mathcal{R}_a}\left(\frac{p}{p_{v_{sat}}(T_w)} - 1\right). \quad (8)$$

Note that the form of equation (7) ensures that $C_w \in [0,1]$. The average bubble temperature is estimated by applying the perfect gas law in a volume averaged sense to the bubble contents,

$$\frac{\bar{T}}{\bar{T}_0} \approx \frac{p\bar{\rho}_0}{p_0\bar{\rho}}, \quad (9)$$

$$\approx \frac{p}{p_0}\frac{R^3}{R_0^3}\frac{m_{a_0} + m_{v_0}}{m_{a_0} + m_v}, \quad (10)$$

where m_{a_0} and m_{v_0} are the initial masses of non-condensible gas and vapor in the bubble, and $R_0 \equiv 1$ has been written for clarity. Results from full computations have shown this approximation to be extremely accurate. The mass of vapor in the bubble, m_v, is determined by integrating,

$$\frac{dm_v}{dt} = 4\pi R^2\dot{m}_v'', \quad (11)$$

where $\dot{m}_v''$ is given by equation (2). The average vapor concentration is approximated by,

$$\bar{C} \approx \frac{m_v}{m_{a_0} + m_v}. \quad (12)$$

The set of model equations (1) through (12), are now closed as long as we have a means of estimating the average transfer coefficients.

We now appeal to some results from linear analysis to develop a simple method for determining the transfer coefficients for a given circumstance. From linear analysis of the diffusion equations in the frequency domain, we can write,

$$\left.\frac{\partial \hat{X}'}{\partial y}\right|_{y=1}(\omega) = -\Psi(\omega; Pe)\hat{\bar{X}}'(\omega), \tag{13}$$

where primes denote small fluctuations, the overbar denotes a quantity averaged over the bubble volume, and $\hat{X}(\omega)$ is the Fourier transform of $X(t)$, which represents either T or C. The transfer function $\Psi(\omega; Pe)$ is,

$$\Psi(\omega; Pe) = \left\{\left[\sqrt{i\omega Pe}\coth\sqrt{i\omega Pe} - 1\right]^{-1} - \frac{3}{i\omega Pe}\right\}^{-1}, \tag{14}$$

where Pe is either Pe_g or Pe_{a-v}. Since the transfer function depends upon ω the transforming of equation (13) back into the time domain would generally result in a convolution integral, which would be of little use for obtaining estimates for the transfer coefficients, and difficult to evaluate numerically. We circumvent the convolution integral by evaluating the transfer function at the isothermal bubble natural frequency. Under the present non-dimensionalization this simply corresponds to setting $\omega = 1$ in equation (14), which results in the frequency independent transfer function being defined as $\Psi(Pe) \equiv \Psi(1; Pe)$.

In general the transfer function $\Psi(Pe)$ is complex valued, with the phase representing a time lag when equation (13) is transformed back into the time domain. The approximations (4) and (5) do not allow for a phase difference and we therefore neglect the phase of the transfer function and define the average transfer coefficients to be,

$$\beta_T \equiv \Re\{\Psi(Pe_g)\}, \tag{15}$$

$$\beta_C \equiv \Re\{\Psi(Pe_{a-v})\}. \tag{16}$$

We now examine the implications of choosing the bubble natural frequency ($\omega = 1$) at which to evaluate the transfer function. The real part, β, and phase, θ, of the transfer function is plotted in figure 1 as a function of Pe. The points on the upper plot are from POD computations described in the next section. We see in the limit $Pe \ll 1$ that $\beta \to 5$ and $\theta \to 0$. So for this case the transfer function *is* constant *and* real valued, and the transformations from frequency domain to time domain can be carried out exactly. Hence, for linear pertubations the model equations will become exact as Pe_g and $Pe_{a-v} \to 0$. It can be shown that this property will also hold in the more general non-linear case.

Away from the low Pe limit the transfer function is no longer a real valued constant, and the evaluation of the transfer function at a single frequency (and the neglect of the phase difference) will have an impact on the accuracy of the model. Obviously during a general bubble motion there are more than one frequency, so the best that we can do is to pick the dominant one. Simple analysis and full computations demonstrate that the presently

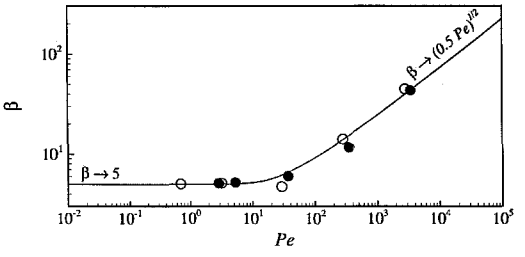

(a) Real Part

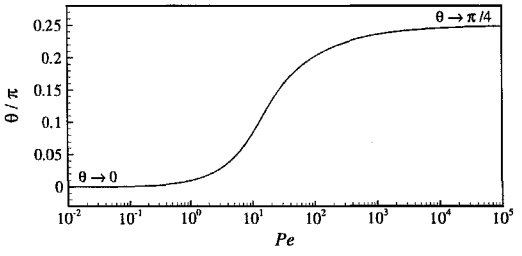

(b) Phase

Figure 1. Real part and phase of transfer function from linear analysis and β from POD analysis: —— Linear analysis; ● POD results from temperature fields; ○ POD results from concentration fields.

used bubble natural frequency is a good representation of the dominant frequency, since the frequency of unforced bubble rebounds scales with the bubble natural frequency. The model can therefore be expected to give the best results possible within the current framework.

FULL COMPUTATIONS

The full computation solves the diffusion equations for the bubble interior using a Chebychev spectral collocation method with an adaptable number of modes (Kamath & Prosperetti 1989, Hao & Prosperetti 1999). Although the full computation is capable of solving the heat and mass diffusion equations in the surrounding liquid, we presently focus our modeling efforts on the bubble interior. Hence all computations presented here neglect the effect of diffusion in the liquid. Comparisons of computations with and without diffusion in the liquid demonstrate the validity of this approximation in the case of air-vapor bubbles in water at (or below) room temperature.

The full computations are a useful tool in the development of reduced-order models. A well known methodology of obtaining such models from full data sets is the application of the *Proper Orthoganal Decomposition* (POD). The goal of the POD in this application is thus; given an ensemble of realizations of a field, $q(y)$, (in this application either the temperature or con-

centration field within the bubble) find the set of POD modes, $\{\phi_k(y)\}_{k=1}^m$, such that the mean projection of q onto ϕ is maximized. The POD computation involves solving a m-dimensional eigen-problem for the POD modes, ϕ_k, and associated eigenvalues, λ_k. Each eigenvalue represents the proportion of "energy" captured by the associated POD mode. Once the POD modes are determined they can be projected onto the governing partial differential equations, which are then reduced to a set of ordinary differential equations. The usefulness of the method hinges on most of the energy being contained within a low number of POD modes so that a low order system results. However, this does not necessarily guarantee success of the method.

To compute the POD we use the method of snapshots developed by Sirovich (1987), where more details on the theory of the POD can also be found. Figure 2 show the first three POD modes for the temperature fields (results for concentration fields look similar) for three typical computations with different values of Pe_g. For the lowest value of Pe_g the POD modes show significant variation over the entire range of y, indicating that the diffusion penetration length is of the same order as the bubble radius. In particular, the first POD mode is well approximated by a quadratic in y, which corresponds to the solution of the diffusion equations in the limit of $Pe_g \to 0$ (Prosperetti 1991). For values of Pe_g lower than this, the POD modes remain essentially unchanged. As Pe_g is increased the POD modes show less variation near the bubble center. Indeed, for $Pe_g = 3475$ in (c), most of the variation in the POD modes is restricted to near the bubble wall, which indicates that the diffusion penetration length is significantly smaller than the bubble radius.

Figure 3 plots the first five eigenvalues for different values of Pe_g. The eigenvalues have been normalized so that their sum is unity. Since the plots indicate such a rapid decay of the eigenvalues with mode number, it is reasonable to use only the first POD mode to obtain a reduced-order model. However, using only one mode is equivalent to using a constant (average) transfer coefficent which may be computed from the first POD mode directly as,

$$\beta \equiv \frac{-\partial\phi_1/\partial y|_{y=1}}{\bar{\phi}_1 - \phi_{1_w}}. \tag{17}$$

This provides direct motivation for the forms of equations (4) and (5) in the development of the model. The transfer coefficients from POD analysis of many full computations over a wide range of Peclet numbers and forcing widths and amplitudes were computed. The values for each Peclet number were averaged, and are superposed on figure 1 for both temperature and concentration distributions. The agreement of these points with the curve from linear theory indicates that the linear theory is an appropriate method to determine the transfer coefficients, which now precludes the need for full computation data and POD analysis.

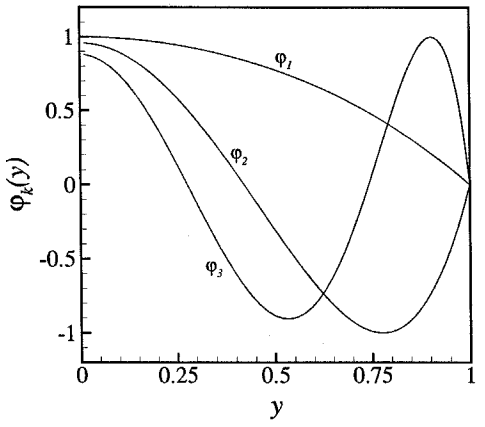

(a) $Pe_g = 36.4$

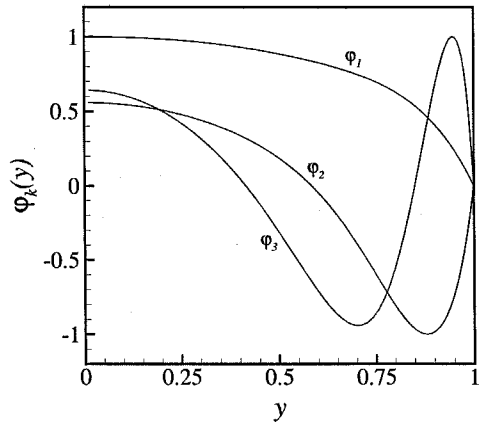

(b) $Pe_g = 349$

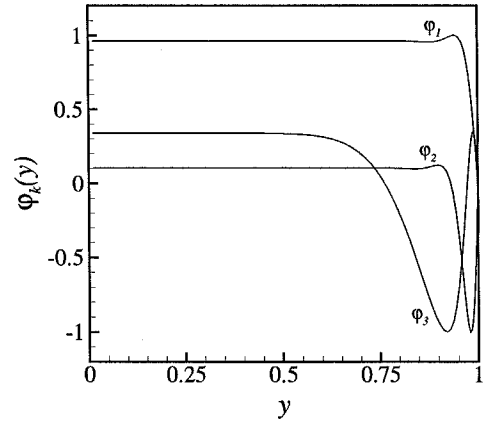

(c) $Pe_g = 3475$

Figure 2. First 3 mode shapes from POD analysis of temperature field data from three full computations with different values of Pe_g.

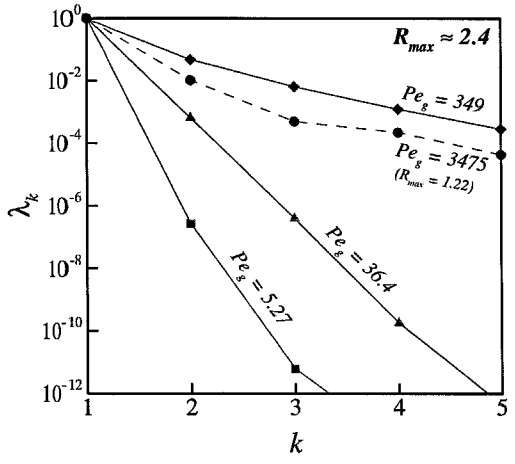

Figure 3. First five normalised eigenvalues from POD analysis for different values of Pe_g.

RESULTS

Gaussian Forcing

The present model is now compared to the full computation and other reduced-order models for single bubbles subjected to the following Gaussian decrease in far field pressure,

$$p_\infty(t) = p_{\infty_o}\left(1 - A\exp\left[-\left((t-t_o)/t_w\right)^2\right]\right), \qquad (18)$$

which has been chosen to approximately represent the pressure that would be experienced by a bubble that is convected through the nozzle of Preston et al. (2002*b*).

Figure 4 compares the different models with a full computation for a typical bubble response. The present model slightly overestimates the initial growth and overdamps the rebounds. However, the present model is superior to the other reduced order models which show greater differences to the full computation. In particular the polytropic model significantly underpredicts the initial bubble growth, due to the effective polytropic index $k_{eff} = 1.21$ being determined from linear analysis (Prosperetti et al. 1988). In reality the time scale for bubble growth is far slower than the time scale that is associated with the bubble natural frequency that was used to compute k_{eff}, so the true behavior is far closer to isothermal, or $k_{eff} = 1$. Interestingly, though the present model also uses the bubble natural frequency to compute transfer coefficients, it is clearly not as sensitive to its value.

The isothermal model makes a better prediction of the slow initial growth than the polytropic model, but in this case the growth is significantly overpredicted. This is likely due to the infinitely fast diffusion of vapor, as explained at the end of this section. There are also problems with the isothermal model that are associated with the use of an effective liquid viscosity,

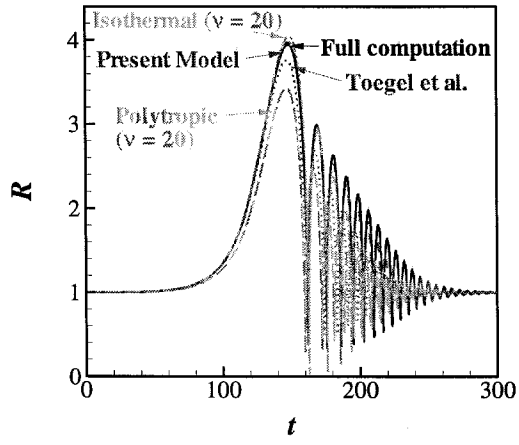

(a) Gross scale

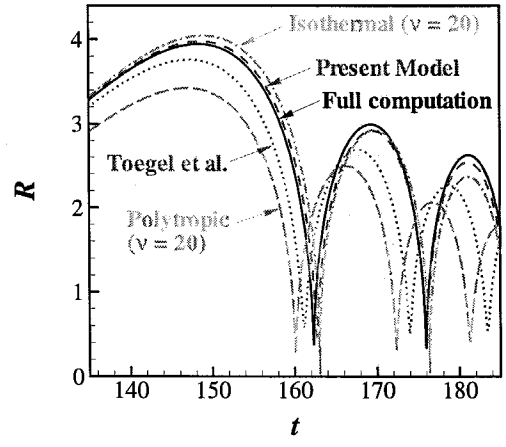

(b) Close up

Figure 4. Bubble radius computed with full computation and a variety of models for a gas-vapor bubble with $Pe_g = 36.4$ and $Pe_{a-v} = 28.8$; Present model ($\beta_T = 6.62$, $\beta_C = 6.21$), model of Toegel et al. (2000), isothermal model ($\nu = 20$), polytropic model ($k_{eff} = 1.21, \nu = 20$).

$\nu \equiv \nu'_{eff}/\nu'_l$, to account for damping due to the otherwise neglected diffusive effects. The value $\nu = 20$ is chosen to match linear analysis (Prosperetti et al. 1988), and works reasonably well for the first bubble rebound in figure 4(b). However, it increasingly overdamps the subsequent rebounds. Furthermore, in other circumstances the same value of effective viscosity results in grossly under attenuated bubble rebounds. This might be corrected by using a higher effective viscosity, but the fact that the appropriate value to use is not known *a priori* is a major limitation of this approach.

The model of Toegel et al. (2000) (and the similar model used by Matula et al. (2002)) uses estimates for the fluxes based upon estimates of the diffusive penetration lengths. The time scale used in their estimates is $t_R \propto R/|\dot{R}|$, which results in the non-realistic situation of low heat and mass transfer during the final stage of collapse and initial rebound when $\dot{R} \approx 0$. While the duration of this non-realistic behavior is so short as to not adversely impact the bubble dynamics, the model has limitations due to the equations not matching the full equations in the limit of low *Pe* (slow time scales) where the diffusion penetration length approaches the size of the bubble. This limitation is evident in figure 4 where the model of Toegel et al. significantly underestimates the initial growth. In addition the model has an error in the treatment of the mass transfer, which results in the incorrect scenario of the mass transfer still being limited by diffusion in the event of the vapor concentration approaching unity. While this error is not substantial for the present plot where bubble growth is moderate and the vapor concentration is not near unity, for large bubble growths (such as those due to the lithotripsy pulses in Matula et al. (2002)) the error becomes significant.

The present model has also been tested for bubbles over a wide range of Peclet number, and forcing widths and amplitudes. In practically all cases the errors in bubble dynamics of the present model are considerably smaller than those of the other reduced-order models. In addition, the estimates of peak bubble pressures and temperatures obtained with the present model, while sometimes only being within an order of magnitude, were consistently better than the other models. The model may therefore be of use in sono-chemistry applications.

Impact of Mass Diffusion

We now examine the importance of modeling mass diffusion by comparing the present model with a model that employs infinitely fast mass diffusion. The model with infinitely fast mass diffusion is derived from the present model by redefining the pressure, p, in equations (1) and (3) to be the partial pressure of non-condensible gas, p_a. The $\dot{m}_v''$ term is removed from equation (1), and the constant vapor pressure $p_{v_{sat}}$ is added to equation (3) to yield,

$$\frac{dp_a}{dt} = \frac{-3\gamma}{R}\left(p_a\frac{dR}{dt} - \frac{p_0}{Pe_g}\frac{1}{R}\frac{\partial T}{\partial y}\bigg|_{y=1}\right), \quad (19)$$

$$p_a + p_{v_{sat}} - p_\infty(t) = R\frac{d^2R}{dt^2} + \frac{3}{2}\left(\frac{dR}{dt}\right)^2 + \frac{4}{ReR}\frac{dR}{dt} + \frac{2}{WeR}. \quad (20)$$

Equations (2) and (11) are then replaced by,

$$m_v = \frac{m_{a_0}}{\theta}, \quad (21)$$

where θ is given by equation (8). The above equation is derived by noting for infinitely fast mass diffusion, $\bar{C} = C_w$, which enables equation (7) and approximation (12) (which is now exact due to the uniform concentration distribution) to be combined.

The bubble radius computed by the full computation and the present model with both finite and infinitely fast mass diffusion is plotted in figure 5(a). It is apparent that infinitely fast mass diffusion results in significant overprediction of the initial bubble growth and subsequent rebounds. The attenuation rate of the rebounds and the bubble minimum radii are also underpredicted. Plots of the average and wall vapor concentrations in figure 5(b) show a higher average vapor concentration for the model with fast mass diffusion, which indicates that the overprediction of the bubble growths is due to too much evaporation into the bubble. The present model with finite diffusion is able to predict the average and wall vapor concentrations remarkably well. It appears that for relatively moderate growth, mass diffusion in the bubble interior is a limiting factor in the bubble growth. The same may not hold true for larger bubble growths where the bubble interior may eventually consist almost entirely of vapor and hence the transport of vapor would not be limited by mass diffusion. In this case the denomenators in equations (2) and (21) would approach zero and the model equations may become singular. In this limit the bubble practically consists of pure vapor with the pressure, p, simply being given by $p_{v_{sat}}$.

Another feature of the solution that is obtained by assuming infinitely fast mass diffusion is the absence of significant vapor content during the fast bubble collapse. Although it is not clear on the scale of figure 5(b) the average vapor concentration during collapse obtained from the model with fast mass diffusion is an order of magnitude lower than it is for the full computation and the present model with finite rate diffusion. It is obvious that the vapor trapping effect identified by Storey & Szeri (2000) is important in this particular circumstance, and the mass diffusion modeling in the present model is able to capture this behavior. This may have important consequences in sonochemistry applications where the amount of vapor trapped in the bubble during collapse would impact on the chemical reactions. In the present application of modeling bubble dynamics the modeling of mass diffusion is important during the collapse stage to avoid the far smaller minimum radii observed in figure 5(a) for the model with fast mass diffusion.

Harmonic Forcing

The present model is intended for application to bubbles exposed to arbitrary pressure excursions that may arise in continuum bubbly model flows. While the previously used Gaussian pressure pulses provide a quick means of testing reduced-order models, it is also useful to test them with harmonic forcings over a wide range of frequencies and amplitudes. We now compare the present model and the often used polytropic model to the full

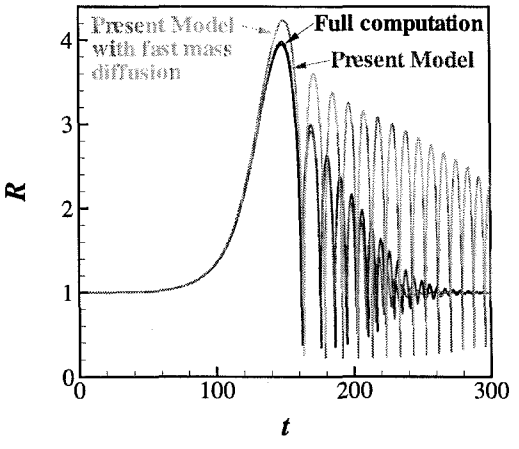

(a) Bubble radius

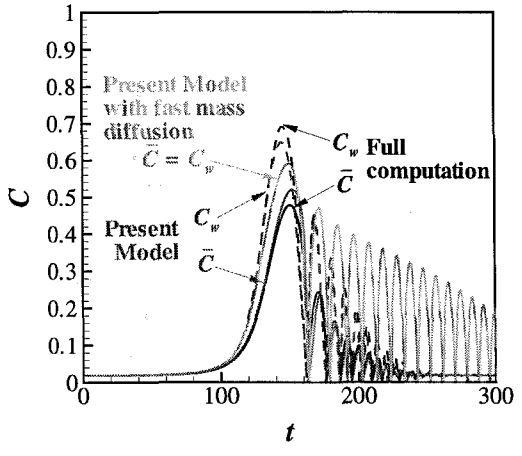

(b) Concentrations

Figure 5. Bubble radius and concentrations computed with full computation and the present model with and without mass diffusion, for a gas-vapor bubble with $Pe_g = 36.4$ and $Pe_{a-v} = 28.8$.

computation for a harmonically forced *pure gas* bubble. The harmonic forcing field is given by,

$$p_\infty(t) = p_{\infty_o}(1 + A\sin\omega_f t), \tag{22}$$

where A is the non-dimensional amplitude and ω_f is the forcing frequency non-dimensionalized by the linear natural bubble frequency.

Figure 6 shows a bifurcation diagram of the computed bubble radius sampled at every period of the forcing, for a bubble with $Pe_g = 9.26$ driven at a forcing frequency $\omega_f = 0.8$ with an incrementally increasing driving pressure amplitude. The curve

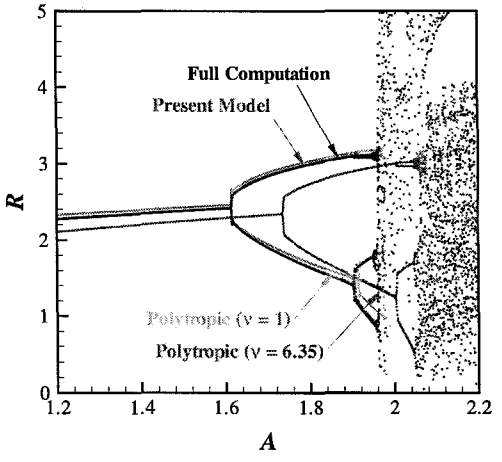

Figure 6. Bifurcation diagram of the bubble radius sampled at every period of the forcing pressure for a gas bubble ($Pe_g = 9.26$) driven with forcing frequency $\omega_f = 0.8$ and a slowly increasing pressure amplitude, A. The curves show comparisons to the full computation of the present model and the polytropic model with and without effective damping ($\nu = 6.35$ and 1 respectively). The effective polytropic index for the polytropic model is $k_{eff} = 1.079$ and heat transfer coefficient for the present model $\beta_T = 5.18$.

for the thermal model is almost identical to the full computation through the first and second subharmonic bifurcations at $A \approx 1.61$ and 1.90. At $A \approx 1.96$ the full computation and thermal model both predict chaotic behavior for which the exact form was found to be very sensitive to tolerances in the numerical integration as well as the rate at which the driving pressure amplitude was increased.

We also compare the thermal model with the polytropic model (using the effective values of polytropic index, k_{eff}, and effective damping, $\nu \equiv \nu'_{eff}/\nu'_L$, obtained to match linear theory (Prosperetti et al. 1988)). The curve for the polytropic model with effective damping ($\nu = 6.35$), while maintaining the same general form as the full computation, is shifted significantly to the right and slightly below the full computation. The polytropic model without effective damping ($\nu = 1$) yields results that agree much more closely with the full computation. It appears that the addition of effective damping to the polytropic model substantially delays the onset of the bifurcations as well slightly overdamps the bubble response.

Figure 7 shows the response of the same bubble forced with non-dimensional pressure amplitude $A = 0.6$ over a range of frequencies. This graph plots (for a given forcing frequency, ω_f) the maximum value of bubble radius attained during a steady oscillation. The thermal model shows excellent agreement to the full computation over all frequencies, even though the model was tuned for forcing at the bubble natural frequency. By contrast, the

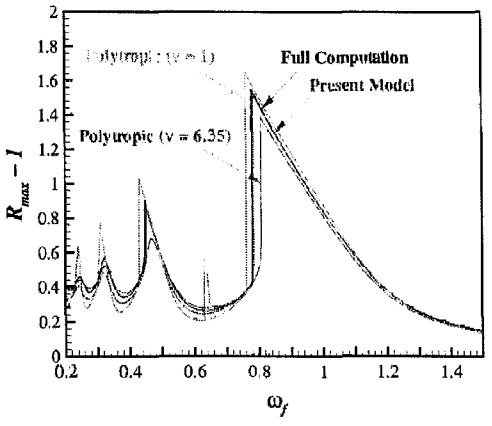

Figure 7. Frequency-response curves for the forced oscillations of a gas bubble ($Pe_g = 9.26$) for a dimensionless pressure amplitude $A = 0.6$. The curves show comparisons to the full computation of the present model and the polytropic model with and without effective damping ($\gamma = 6.35$ and 1 respectively). The effective polytropic index for the polytropic model is $k_{eff} = 1.079$ and heat transfer coefficient for the present model is $\beta_T = 5.18$.

polytropic model is unable to correctly predict the location and magnitude of the harmonic peaks, and the behavior of the model depends strongly on the (arbitrary) value of effective damping that is used.

We also constructed bifurcation diagrams and frequency response curves for a larger bubble ($Pe_g = 42.9$, $\beta_T = 6.96$), which showed similar trends as the plots presented here . For both bubble sizes the present model gives results that agree with the full computation much more closely than the polytropic model with or without effective damping.

CONCLUSION

A simple and efficient model that accounts for diffusive damping effects in gas-vapor bubbles has been presented. The model is motivated by results of POD being applied to data from full computations, which indicated that the use of average heat and mass transfer coefficients would be appropriate. The transfer coefficients are determined from linear analysis, which are shown to agree with those that are obtained from POD. The model has been shown to have better agreement with full bubble computations than other reduced-order models, over a wide range of forcings.

ACKNOWLEDGMENT

This research was supported by NSF under grant number CTS 9979258 and NIH under grant number PO1 DK43881.

REFERENCES

Hao, Y. & Prosperetti, A. (1999), 'The effect of viscosity on the spherical stability of oscillating gas bubbles', *Phys. Fluids* **11**(6), 1309–1317.

Ichihara, M., Kawashima, H. & Kameda, M. (2000), 'Dynamics of a spherical gas/vapor bubble', *Proceedings of the Third Annual Meeting of the Institute for Multifluid Science and Technology (IMuST)*.

Kamath, V. & Prosperetti, A. (1989), 'Numerical integration methods in gas-bubble dynamics', *J. Acoust. Soc. Am* **85**(4), 1538–1548.

Kameda, M. & Matsumoto, Y. (1996), 'Shock waves in a liquid containing small gas bubbles', *Phys. Fluids* **8**(2), 322–355.

Lin, H., Storey, B. D. & Szeri, A. J. (2002), 'Inertially driven inhomogeneities in violently collapsing bubble: the validity of the rayleigh-plesset equation', *J. Fluid Mech.* **452**, 145–162.

Matsumoto, Y. & Takemura, F. (1994), 'Influence of internal phenomena on gas bubble motion', *JSME International Journal Series B-Fluids and Thermal Engineering* **37**(2), 288–296.

Matula, T. J., Hilmo, P. R., Storey, B. D. & Szeri, A. J. (2002), 'Radial response of individual bubbles subjected to shock wave lithotripsy pulses *in vitro*', *Phys. Fluids* **14**(3), 913–921.

Nigmatulin, R. I., Khabeev, N. S. & Nagiev, F. B. (1981), 'Dynamics, heat and mass transfer of vapour-gas bubbles in a liquid', *Int. J. Heat Mass Transfer* **24**(6), 1033–1044.

Preston, A., Colonius, T. & Brennen, C. E. (2002*a*), 'A reduced-order model of heat transfer effects on the dynamics of bubbles', *ASME FEDSM'02*.

Preston, A. T., Colonius, T. & Brennen, C. E. (2002*b*), 'A numerical investigation of unsteady bubbly cavitating nozzle flows', *Phys. Fluids* **14**(1), 300–311.

Prosperetti, A. (1991), 'The thermal behaviour of oscillating gas bubbles', *J. Fluid Mech.* **222**, 587–616.

Prosperetti, A., Crum, L. A. & Commander, K. W. (1988), 'Nonlinear bubble dynamics', *J. Acoust. Soc. Am.* **83**(2), 502–514.

Sirovich, L. (1987), 'Turbulence and the dynamics of coherent structures, parts i-iii', *Q. Appl. Math* **XLV**(3), 561–590.

Storey, B. D. & Szeri, A. J. (2000), 'Water vapour, sonoluminescence and sonochemistry', *Proc. R. Soc. Lond. A* **456**, 1685–1709.

Storey, B. D. & Szeri, A. J. (2001), 'A reduced model of cavitation physics for use in sonochemistry', *Proc. R. Soc. Lond. A* **457**, 1685–1700.

Toegel, R., Gompf, B., Pecha, R. & Lohse, D. (2000), 'Does water vapor prevent upscaling sonoluminescence?', *Phys. Rev. Lett.* **85**(15), 3165–3168.

Watanabe, M. & Prosperetti, A. (1994), 'Shock waves in dilute bubbly liquids', *J. Fluid Mech.* **274**, 349–381.